Bulletin of the Seismological Society of America, Vol. 96, No. 3, pp. 898–913, June 2006, doi: 10.1785/0120050122

Attenuation Relations of Strong Ground Motion in Japan Using Site Classification Based on Predominant Period

by John X. Zhao, Jian Zhang, Akihiro Asano, Yuki Ohno, Taishi Oouchi, Toshimasa Takahashi, Hiroshi Ogawa, Kojiro Irikura, Hong K. Thio, Paul G. Somerville, Yasuhiro Fukushima, and Yoshimitsu Fukushima

Abstract A spectral acceleration attenuation model for Japan is presented in the present study. The data set includes a very large number of strong ground-motion records up to the 2003 Off Tokach main and aftershocks. Site class terms, instead of individual site correction terms, are used. The site classes of recording stations are from a recent study on site classification for strong-motion recording stations in Japan according to a classification scheme that has been used in Japanese engineering design. The use of site class terms enables tectonic source-type effects to be identified and accounted for in the present model. The effects of a faulting mechanism for crustal earthquakes also are accounted for. For crustal and interface earthquakes, a simple form of an attenuation model (with respect to distance) is able to capture the main strong-motion characteristics and achieves unbiased estimates. For subduction slab events, a simple distance modification factor is employed to achieve plausible and unbiased predictions. The effects of source depth, tectonic source type, and faulting mechanism of crustal earthquakes are significant. The need for magnitude-squared terms is evaluated, and the use of magnitude-squared terms reduces the interevent error further.

Introduction

Many attenuation relations for strong ground motion have been developed as an important component of seismic hazard studies. In a deterministic manner engineers also use attenuation models to estimate the forces and/or displacements induced in engineering structures. In probabilistic seismic hazard analysis, both the mean values and the prediction uncertainties of an attenuation model are utilized, and high model prediction uncertainties can lead to high probabilistic ground-motion estimates at long return periods.

Japan is located in an active plate boundary environment and, therefore, has a complicated geological and tectonic setting. Because the seismic wave propagating paths from earthquake source to the ground surface vary from one type of earthquake to another, the ground motions generated by different types of earthquakes are expected to be different even if the events have identical magnitudes and source distances. In the past, spectral attenuation models developed for earthquakes in Japan have not usually accounted for tectonic source type, though different attenuation characteristics between interface and slab events have been widely recognized (see Morikawa and Sasatani, 2004).

The site conditions at a recording station have a very strong influence on ground motions induced by earthquakes. A significant effort has therefore been made to collect and assess the geotechnical information of recording stations. Until now, the majority of the strong-motion stations in Japan have had limited geotechnical information. Many researchers in Japan have attempted to overcome this difficulty by assigning individual site terms for each recording station (Fukushima and Tanaka, 1990; Molas and Yamazaki, 1995; Kobayashi, *et al.*, 2000; Takahashi *et al.*, 2004). Possible drawbacks to this approach are that the regression systems have too many terms to determine and that the model's prediction error and some of the source effects may propagate into individual site terms (Zhao *et al.*, 2004). However, the use of generic soil effect terms for each soil category based on the reasonably reliable site classes assigned by Zhao *et al.* (2004) avoids using too many terms for each group of the recording sites, and we are able to evaluate the effects of tectonic source type and faulting mechanism for crustal earthquakes.

Strong-Motion Data Set

Figure 1a shows the magnitude and source distance (defined in equations 1 and 2 in the next section) distribution for earthquakes with focal depths of up to 162 km for the Japanese strong-motion data set, and Figure 1b shows that

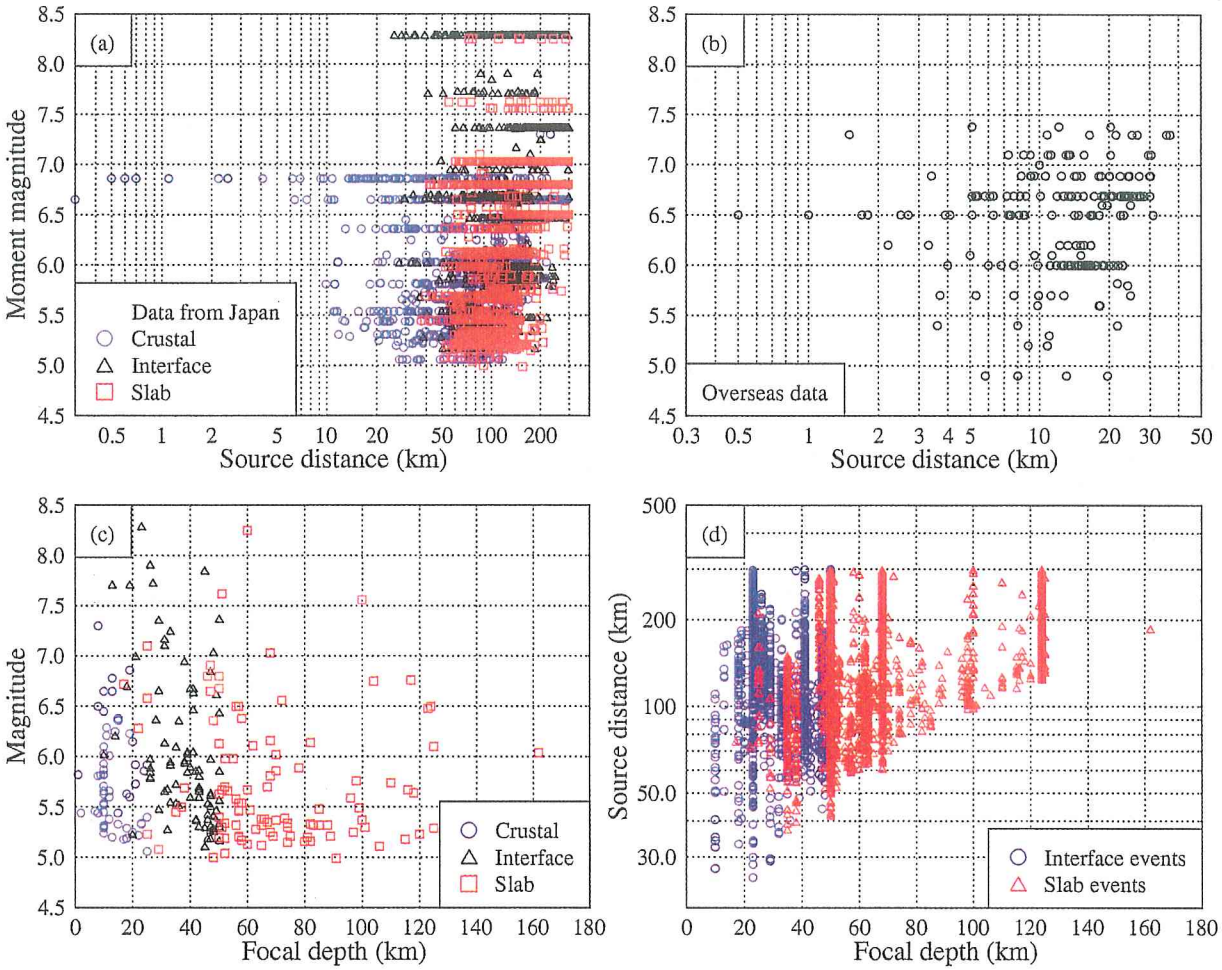

Figure 1. Magnitude-distance distribution for (a) data from Japan; (b) overseas data; (c) magnitude-focal depth distribution; and (d) source distance-focal depth distribution of Japanese data.

of the overseas data sets used in the modeling. In order to eliminate the bias possibly introduced by untriggered instruments, data for the modeling were selected from a much larger data set by exclusion of data at distances larger than a specified value for a given magnitude (see Fig. 1a). For subduction slab events, the maximum source distance was set to 300 km. There are only a small number of records within 30-km source distance in the Japanese data set, and all near-source data within 10 km is from the 1995 Kobe earthquake and the 2000 Tottori earthquake. The overseas data from the western part of the United States and the 1978 Tabas, Iran, earthquake provide a small but valuable amount of additional data within the 40-km source distance, and these records were used primarily to constrain the near-source behavior of the model. The overseas near-source data represent the "missing" data in the Japanese data set, and the inclusion of the overseas near-source data would have a relatively small effect on model prediction error caused by using "incomplete" data from these events, in other words, the distant data from these earthquakes were not used. The interevent error (see subsequent section) may be affected by the overseas earthquakes (compared with the scenario in which the near-source data from Japan are from the same events that have been already included), but the effect is likely to be small as only 20 overseas events were used out of a total of 269 earthquakes. Figure 1c shows the magnitude and focal depth distributions for the Japanese data. There is a reasonably good distribution of data for all magnitude and focal depth ranges, and the records from deep slab events provide good constraint to the depth term of the attenuation model. The maximum depth for crustal earthquakes was set to 25 km, and 50 km for interface events. Figure 1d shows a strong correlation between focal depth and source distance, because focal depth contributes to the distance, especially for slab events. We found that the epicentral latitudes and longitudes and focal depths determined by the Japan Meteorological Agency were not consistent with those determined by other seismological organizations. For example, zero depth was assigned when the focal depth could not be reliably evaluated. We used the relocated International Seis-

mological Centre (ISC) locations and depths (Engdahl *et al.*, 1998) in the present study because an early study (Kobayashi *et al.*, 2000) found that interevent residuals were reduced significantly by using the relocated ISC locations and depths. The moment magnitudes are from the Harvard catalogue unless moment magnitude from a special study is available.

Subduction slab and interface events were identified manually by plotting events and their mechanisms in a vertical cross section through the subduction zone, perpendicular to the trench, at the relevant location. Interface events were identified both by their proximity to the subduction zone interface and the alignment of their mechanism with the prevailing dip of the interface. The differentiation in focal mechanism was based on a rake angle criterion, with a rake of ± 45 as demarcation between dip-slip and strike-slip. For a very few events, we adjusted these bounds slightly based on the overall mechanism and tectonic environment.

Table 1 shows the breakdown of record numbers by source type and focal mechanism categories. Among the total of 4518 Japanese records, 1285 are from crustal events, 1508 are from interface events, and 1725 are from slab events. For crustal events, many published attenuation models show that events with reverse-faulting mechanisms produce higher ground motions than strike-slip events. The number of records from reverse-fault events is large enough for the present study to account for the possible difference between the ground motions from reverse and strike-slip events (see Table 1). The very small number of records from crustal events with normal faulting mechanisms does not warrant the normal-fault events being considered as a separate group.

Nearly all available records from earthquakes with source type, focal mechanism, and moment magnitude available since 1968 in Japan have been included in the present study. The number of records from each event varies greatly, not only for older events but also for earthquakes up to the late 1990s. However, any undesirable effect of the uneven distribution of records among earthquakes should be largely eliminated by the random effects model, which separates the model prediction error into inter- and intra-event parts.

The data from the western part of the United States are all from crustal earthquakes (except for a 25 April 1992 event that was identified as an interface event) with focal depths less than 20 km. Of the total of 196 near-source records from crustal earthquakes, 123 records are from reverse-faulting events, and 73 records are from strike-slip events. For the overseas interface event, 12 near-source records were used. The locations of these events are from the Hauksson (2000) catalogue. Records at short source distances from large subduction earthquakes in Mexico and Chile were not included, primarily because the Mexico subduction zone was characterized as a "weak" coupling zone, and the Chilean subduction zone was characterized as a "strong" coupling zone (Kanamori, 1986), representing the two extreme ends of subduction zone characteristics, and the characteristics of the subduction earthquakes in these two areas may be very different from those in Japan.

All records from Japan have been processed in a consistent manner. First, instrumental response was corrected, and this proved to be a huge task, as there are many different types of instruments. The second step was to select the usable period range. For the short-period end, we used a low-pass filter to eliminate ground motions over 24.5 Hz for those records with a 50-Hz sampling rate and 33 Hz for records with a 100-Hz sampling rate. The spectra at short periods and even peak ground acceleration (PGA) were not noticeably affected by the low-pass filter (PGA is actually associated with ground motions with frequencies between 2 and 5 Hz for most records used in the present study). Determination of the long-period end of the usable period range was difficult. For many records, instruments were triggered by *P*-wave arrivals, and there were no pretrigger recordings that may be used as the recorded instrument and site noise. A simple and efficient processing method was used in the present study:

Table 1
Numbers of Records by Source Type, Faulting Mechanism, and Region

Focal Mechanism	Crustal	Interface	Slab	Total for Each Focal Mechanism
Japan				
Reverse	250	1492	408	2150
Strike-slip	1011	13	574	1598
Normal	24	3	735	762
Unknown			8	8
Total for each source type	1285	1508	1725	4518
Iran and Western USA				
Reverse	123	12		135
Strike-slip	73			73
Total for each source type	196	12		208
Totals for each source type from all regions				Grand Total
	1481	1520	1725	4726

1. Acceleration time histories were visually inspected to detect any faulty recordings, *S*-wave triggers, or recordings from multi-events.
2. If a record had relatively large values at the beginning (*P* wave) and the end of the record, the record was mirrored and tapered for 5 sec at each end of the record.
3. Five seconds of zeros was appended at both the beginning and the end of an acceleration record and calculating displacement time history in the frequency domain;
4. The displacement amplitude in the time range of the padded zeros was compared with the peak displacement within the duration of the actual record, and if the displacement amplitude in the time range padded with zeros was relatively large, a high-pass filter was used to eliminate the motion at low frequencies.
5. The corner frequency f_c of the high-pass filter was increased to a value until the displacement amplitude in the time range of the padded zeros was "small" (subjective judgement) and the period of $1/f_c$ was the maximum usable period.

The theoretical background of this method is that, if the Fourier spectrum of a displacement time-history has high amplitude at low frequencies (for example, increasing with decreasing frequency, instead of "flat"), the relative high amplitude of the displacement Fourier spectrum at low frequencies can be approximated by a constant Fourier spectral "block." In the time domain the high-amplitude constant Fourier spectral block will produce a pulse (delta-function type) that will have a considerably large displacement amplitude in the beginning and end of the record where the signal is supposed to be zero. This processing procedure does not need the noise level of a recorder or a site, and the processing is very efficient. The method was verified by processing records from K-net stations that contained a 10-sec pre-*P*-arrival recording used as the noise level. The high-pass filtering reduced the number of Japanese records from 4518 records at 0- to 1.0-sec periods to 2763 at the 5-sec period. The maximum periods for the United States and Iran data were adopted from overseas processing agencies (primarily California Strong Motion Instrumentation Program [CSMIP]).

Four site classes are used in the present study, SC I, II, III and IV, approximately corresponding to the four classes, rock, hard soil, medium soil, and soft soil, as defined by Molas & Yamazaki (1995). See also Table 2, which shows the approximately corresponding site classes defined by the Building Seismic Safety Council (2000). Table 3 shows the distribution of the number of data in each site class, and nearly all records used are from the free field or the basements of small structures. A few records from instruments mounted at shallow depth in very strong bed rock were also included.

Development of the Base Model

In the present study, the random-effects model is adopted and the algorithm of Abrahamson and Youngs (1992) is used. The following simple form of the attenuation function was selected:

$$\log_e(y_{i,j}) = aM_{wi} + bx_{i,j} - \log_e(r_{i,j}) + e(h - h_c)\,\delta_h + F_R + S_I + S_S + S_{SL}\log_e(x_{i,j}) + C_k + \xi_{i,j} + \eta_i, \quad (1)$$

$$r_{i,j} = x_{i,j} + c\exp(dM_{wi}), \quad (2)$$

where y is either PGA (in centimeters per second^2) or 5% damped acceleration response spectrum (the geometric mean of two horizontal components in centimeters per second^2) for a spectral period T, M_w is the moment magnitude, x is the source distance in kilometers, and h is the focal depth in kilometers. The reverse-fault parameter F_R applies only to crustal events with a reverse-faulting mechanism and is zero for all other events. The tectonic source-type parameter S_I applies to interface events and is 0 for all other type events, and S_S applies to subduction slab events only and is zero for all other type events. S_{SL} is a magnitude-independent path modification term for slab events to account for the complex seismic wave travel path for slab events. C_k is the site-class term for a given site class. Subscript i denotes event number and j denotes record number from event i. Coefficient h_c is a depth constant. When h is larger than h_c, the depth term $e(h - h_c)$ takes effect, with δ_h being a dummy variable that equals 0 for $h < h_c$ and 1 for $h \geq h_c$. When h is larger than 125 km, $h = 125$ km is selected so that a constant factor is used for deeper earthquakes (i.e., depth is capped at 125 km). Random variable η_{ij} is the intra-event error (error that represents the variability from the median predicted value for a

Table 2
Site Class Definitions Used in the Present Study and the Approximately Corresponding NEHRP Site Classes

Site Class	Description	Natural Period	V_{30} Calculated from Site Period	NEHRP Site Classes
Hard rock			$V_{30} > 1100$	A
SC I	Rock	$T < 0.2$ sec	$V_{30} > 600$	A + B
SC II	Hard soil	$0.2 = T < 0.4$ sec	$300 < V_{30} = 600$	C
SC III	Medium soil	$0.4 = T < 0.6$ sec	$200 < V_{30} = 300$	D
SC IV	Soft soil	$T = 0.6$ sec	$V_{30} = 200$	E + F

Table 3
Numbers of Records by Site Class and Source Type

Source Type	Unknown	SC I	SC II	SC III	SC IV	Total for Each Source Type
Japan						
Crustal	32	427	401	137	288	1285
Interface	9	373	540	186	400	1508
Slab	22	668	530	210	295	1725
Total for each site class	63	1468	1471	533	983	4518
Iran and Western USA						
Crustal		24	73	93	6	196
Interface		2	7	3		12
Total for each site class		26	80	96	6	208
Totals for each site class from all regions	63	1494	1551	629	989	Grand Total 4726

particular recording station in a given event) with zero mean and a standard deviation of σ, and random variable η_i is interevent error (error that represents variability between earthquakes of the same magnitude) with zero mean and a standard deviation of τ. Coefficients a, b, c, d, and e, site class term C_k, reverse-fault term F_R, and source-type terms S_I S_S, and S_{SL} are determined by regression analysis for each period. Source distance x is the shortest distance to the rupture zone for earthquakes with available fault models, and hypocentral distance for the other events.

The coefficients of the simple model in equation (1) were derived from the data set, and extensive analyses on inter- and intra-event residuals were then carried out. The results of our analyses suggested that the simple model in equation (1) predicts spectral accelerations that are reasonably unbiased over magnitude and distance for crustal and interface events, and not seriously biased for slab events, even when the coefficients of the magnitude, geometric spreading, and anelastic attenuation terms are the same for all three types of events. The modification factor for slab events applies only to a source distance of about 40 km or larger, because the term $-\log_e(x_{ij})$ in equation (1) monotonically increases with decreasing source distance, but this should pose no restrictions to most practical applications.

The total standard error of the model's prediction is defined by

$$\sigma_T = \sqrt{\sigma^2 + \tau^2}. \quad (3)$$

Both intra- and interevent errors σ and τ are period dependent but are assumed independent of magnitude.

We used the value of 15 km for the depth coefficient h_c in the present study, as this value appears to have the best depth effect for shallow events (with depth <25 km). Positive and statistically significant estimates for the depth coefficient e were achieved for all periods.

The coefficients of all the terms in equations (1) and (2) are shown in Tables 4 and 5. They differ moderately from those of the Takahashi *et al.* (2004) model. However the predicted spectra for much of the magnitude and distance range of the present model are similar to those predicted by the Takahashi *et al.* (2004) model. The differences possibly result from changes in coefficient c for slightly improved model prediction at a short source distance and the inclusion of over 300 records from the M_w 8.3 interface event (26 September 2003). Note that the coefficients in Table 1 have not been smoothed with respect to spectral period, and no constraints have been imposed on any of the coefficients apart from checking whether a coefficient is statistically significant. The anelastic attenuation rates at 4- and 5-sec periods are larger than those at a 3-sec period, and this is presumably the result of the rapid reduction in the number of records with increasing period, due to the elimination of long-period recording noise level. A side effect of equation (1) is the assumption of identical anelastic attenuation rates for all earthquakes. The seismic waves generated by subduction slabs with a depth of 50 km or more may experience less anelastic attenuation than those from shallow earthquakes, and the effect of assuming identical anelastic attenuation rate for deep slab events to that of shallow events may be partially offset by the additional geometric attenuation term for slab events. The assumption of identical anelastic attenuation rates for all earthquakes may also cause variation in the anelastic attenuation rate in a manner that is not consistent with the physical understanding of the anelastic attenuation.

In some of the following comparisons with the models from other studies, a "mean model" is used to overcome the differences in site classification schemes. The mean model refers to that for which the F_R, S_L, S_S, and S_{SL} terms in equation (1) are all zero (i.e., strike-slip or normal crustal earthquakes) and the site term takes the mean value C_M (mean site conditions), as calculated in equation (4),

$$C_M = \frac{C_I N_I + C_{II} N_{II} + C_{III} N_{III} + C_{IV} N_{IV} + C_{ID} N_{ID}}{N_I + N_{II} + N_{III} + N_{IV} + N_{ID}}, \quad (4)$$

Table 4
Coefficients for Source and Path Terms of the Models in the Present Study

Period (sec)	a	b	c	d	e	S_R	S_I	S_S	S_{SL}
PGA	1.101	−0.00564	0.0055	1.080	0.01412	0.251	0.000	2.607	−0.528
0.05	1.076	−0.00671	0.0075	1.060	0.01463	0.251	0.000	2.764	−0.551
0.10	1.118	−0.00787	0.0090	1.083	0.01423	0.240	0.000	2.156	−0.420
0.15	1.134	−0.00722	0.0100	1.053	0.01509	0.251	0.000	2.161	−0.431
0.20	1.147	−0.00659	0.0120	1.014	0.01462	0.260	0.000	1.901	−0.372
0.25	1.149	−0.00590	0.0140	0.966	0.01459	0.269	0.000	1.814	−0.360
0.30	1.163	−0.00520	0.0150	0.934	0.01458	0.259	0.000	2.181	−0.450
0.40	1.200	−0.00422	0.0100	0.959	0.01257	0.248	−0.041	2.432	−0.506
0.50	1.250	−0.00338	0.0060	1.008	0.01114	0.247	−0.053	2.629	−0.554
0.60	1.293	−0.00282	0.0030	1.088	0.01019	0.233	−0.103	2.702	−0.575
0.70	1.336	−0.00258	0.0025	1.084	0.00979	0.220	−0.146	2.654	−0.572
0.80	1.386	−0.00242	0.0022	1.088	0.00944	0.232	−0.164	2.480	−0.540
0.90	1.433	−0.00232	0.0020	1.109	0.00972	0.220	−0.206	2.332	−0.522
1.00	1.479	−0.00220	0.0020	1.115	0.01005	0.211	−0.239	2.233	−0.509
1.25	1.551	−0.00207	0.0020	1.083	0.01003	0.251	−0.256	2.029	−0.469
1.50	1.621	−0.00224	0.0020	1.091	0.00928	0.248	−0.306	1.589	−0.379
2.00	1.694	−0.00201	0.0025	1.055	0.00833	0.263	−0.321	0.966	−0.248
2.50	1.748	−0.00187	0.0028	1.052	0.00776	0.262	−0.337	0.789	−0.221
3.00	1.759	−0.00147	0.0032	1.025	0.00644	0.307	−0.331	1.037	−0.263
4.00	1.826	−0.00195	0.0040	1.044	0.00590	0.353	−0.390	0.561	−0.169
5.00	1.825	−0.00237	0.0050	1.065	0.00510	0.248	−0.498	0.225	−0.120

Table 5
Coefficients for Site Class Terms and Prediction Error

Period (sec)	C_H	C_1	C_2	C_3	C_4	σ	τ	σ_T
PGA	0.293	1.111	1.344	1.355	1.420	0.604	0.398	0.723
0.05	0.939	1.684	1.793	1.747	1.814	0.640	0.444	0.779
0.10	1.499	2.061	2.135	2.031	2.082	0.694	0.490	0.849
0.15	1.462	1.916	2.168	2.052	2.113	0.702	0.460	0.839
0.20	1.280	1.669	2.085	2.001	2.030	0.692	0.423	0.811
0.25	1.121	1.468	1.942	1.941	1.937	0.682	0.391	0.786
0.30	0.852	1.172	1.683	1.808	1.770	0.670	0.379	0.770
0.40	0.365	0.655	1.127	1.482	1.397	0.659	0.390	0.766
0.50	−0.207	0.071	0.515	0.934	0.955	0.653	0.389	0.760
0.60	−0.705	−0.429	−0.003	0.394	0.559	0.653	0.401	0.766
0.70	−1.144	−0.866	−0.449	−0.111	0.188	0.652	0.408	0.769
0.80	−1.609	−1.325	−0.928	−0.620	−0.246	0.647	0.418	0.770
0.90	−2.023	−1.732	−1.349	−1.066	−0.643	0.653	0.411	0.771
1.00	−2.451	−2.152	−1.776	−1.523	−1.084	0.657	0.410	0.775
1.25	−3.243	−2.923	−2.542	−2.327	−1.936	0.660	0.402	0.773
1.50	−3.888	−3.548	−3.169	−2.979	−2.661	0.664	0.408	0.779
2.00	−4.783	−4.410	−4.039	−3.871	−3.640	0.669	0.414	0.787
2.50	−5.444	−5.049	−4.698	−4.496	−4.341	0.671	0.411	0.786
3.00	−5.839	−5.431	−5.089	−4.893	−4.758	0.667	0.396	0.776
4.00	−6.598	−6.181	−5.882	−5.698	−5.588	0.647	0.382	0.751
5.00	−6.752	−6.347	−6.051	−5.873	−5.798	0.643	0.377	0.745

where C is the site term and N is the number of records in each site class, with subscripts I, II, III, and IV for site classes I, II, II, and IV, respectively. C_{ID} is the mean value of the individual site terms (for those sites with 3 or more records but without site classes), and N_{ID} is the total number of sites with individual site terms.

Twelve SC I stations, which yielded 93 records, are rock sites having average shear-wave velocities in the range 1020–2200 m/sec mostly measured by refraction seismic profiling and *P-S* logging. They are referred to as hard rock sites in the present study. The average intra-event residuals were found to decrease with increasing shear-wave velocity for all periods. Assuming that the average shear-wave velocity of all SC I sites is 700 m/sec (a very large portion of SC I sites have a layer of soil on soft rock, and the selection of 700 m/sec as average is likely to be reasonable), a function having a linear term $\log_e (V_s/700)$ where V_s is in m/sec, and a fourth-order polynomial of $\log_e(T)$ term where T is spectral

period, was fitted to the intra-event residuals from the hard rock sites. This allows the site term for hard rock sites to be calculated by adding the predicted intra-event residuals for a given period and shear-wave velocity to the corresponding site terms for SC I sites. As an example, the hard rock site terms C_H are presented in Table 5 for hard rock sites with V_S = 2000 m/sec, together with all other coefficients. Because of the small number of records from hard rock sites, further interpretation of the hard rock site terms may not be warranted.

One feature of equation (1) is that all three source types have the same magnitude scaling and the same near-source characteristics (identical coefficients *a*, *c*, and *d*). Residual analyses showed that the same magnitude scaling captures the first-order effect reasonably well, that is, the interevent residuals do not have a large linear trend with respect to magnitude. However, the magnitude-squared terms introduced later reveal that different magnitude scaling for different earthquake source types leads to a sizeable reduction in interevent error. The near-source data were nearly all from crustal earthquakes, apart from a dozen or so records from interface events within 20 km. The near-source behavior for subduction models is largely constrained by the records from crustal events, and we do not expect that the model prediction over 30 km for subduction earthquakes would be affected by this constraint. We do not consider this constraint to be theoretically sound, but the implication to the application of the attenuation models for subduction events in Japan is minimal because the minimum source distance from a site on land to the rupture plane for any subduction event would probably be 30 km or more in most cases.

The PGAs predicted by the crustal and interface models are compared with data from crustal and interface earthquakes of magnitude 6.0 or larger in Figure 2a and b, respectively. The PGA data have been normalized to magnitude 7.0, a focal depth of 20 km, crustal events with strike-slip mechanism, and SC II site conditions. The model fits this subset of the data reasonably well, especially the near-source data from SC I and II sites, in the source distance range of 0–10 km, including data recorded in the Kobe 1995 earthquake. A few records of earthquakes in the western part of the United States are reasonably well predicted. The near-source records that were overpredicted are from SC III and IV sites where nonlinear response was considered to be substantial (among those were the near-source records from the 1995 Kobe earthquake as reported by Fukushima *et al.* [2000]). The predicted PGAs of slab models are compared with the normalized PGAs from subduction slab events in Figure 2c.

Figure 3 shows a comparison with PGAs predicted by the models of Fukushima *et al.* (2000) and Si and Midorikawa (1999). Note that the Si and Midorikawa (1999) model is for the larger of the two horizontal components, so the predicted values of their models were divided by 1.13, which was the average ratio of the larger of and the geometric mean of the two horizontal components for PGA in our data set.

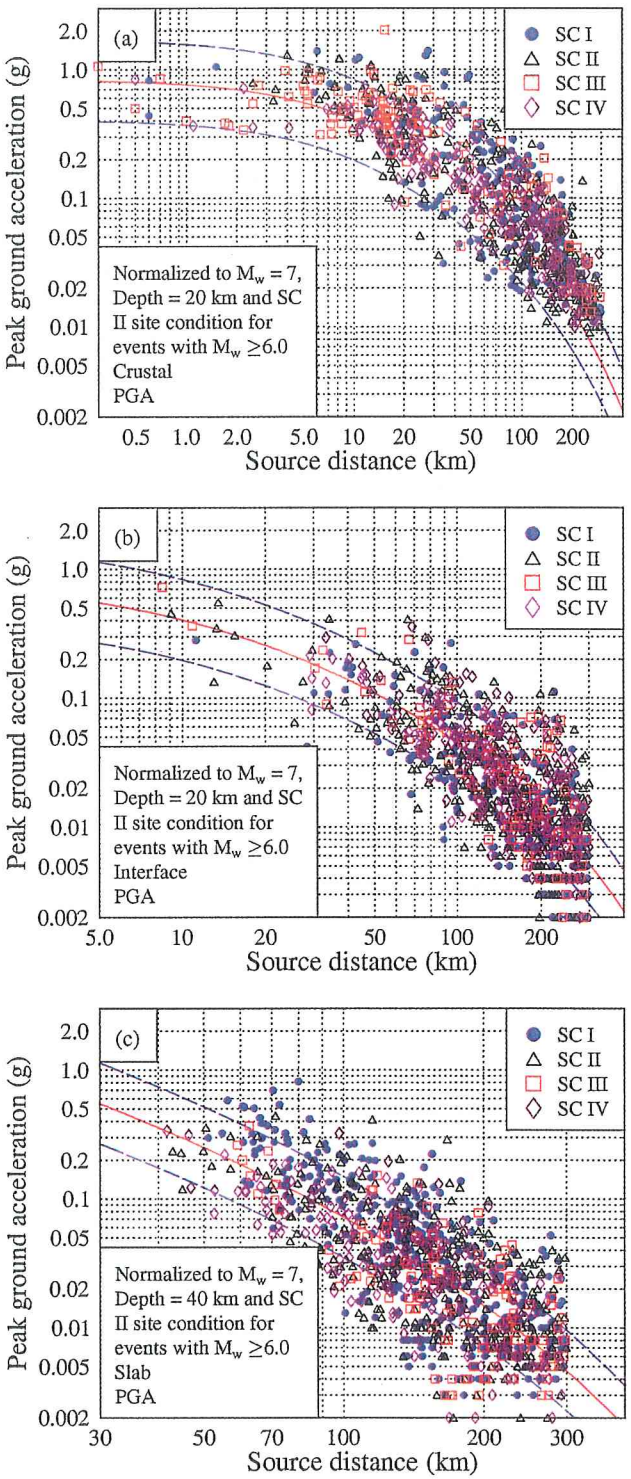

Figure 2. Comparison of predicted PGA by the present model with the PGAs from earthquakes with magnitude 6.0 or larger, for (a) crustal, (b) interface, and (c) slab events. The PGAs have been normalized to M_w 7.0 at a focal depth of 30 km for SC II site conditions.

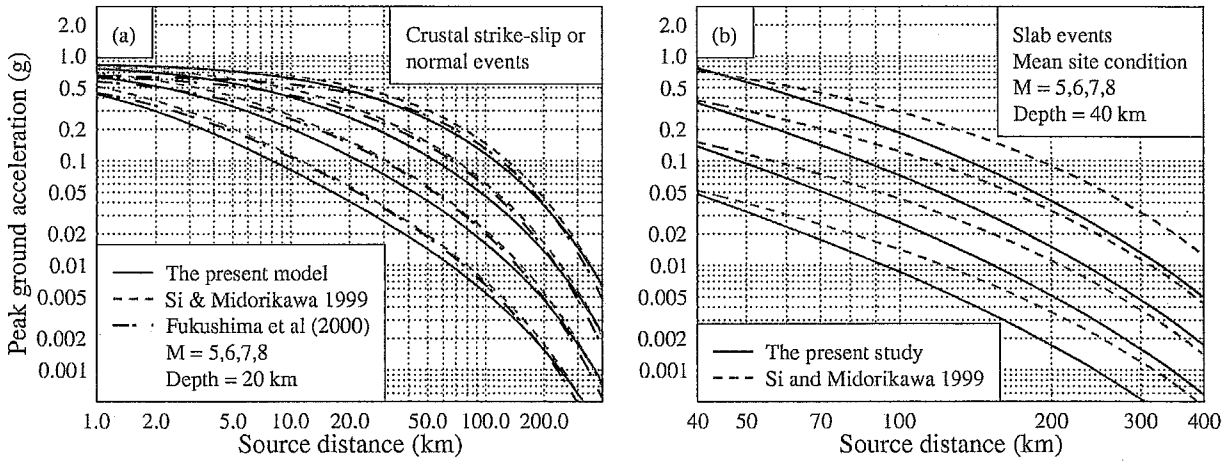

Figure 3. Comparison of predicted PGA by the present model with those of (a) Fukushima *et al.* (2000) and Si and Midorikawa (1999) for crustal strike-slip events and (b) Si and Midorikawa for slab events, with the mean site terms for magnitudes 5, 6, 7, and 8.

At all magnitudes, the crustal and interface models derived in the present study predict reasonably similar PGAs to those predicted by the Fukushima *et al.* (2000) model over reasonably large magnitude and distance ranges (Fig. 3a) for mean site conditions. The Si and Midorikawa (1999) models for crustal and interface earthquakes predict generally larger PGAs than those by the present model. At a small source distance (<0.2 km) for M_w 7.0, the present model predicts a PGA of about 0.8 g, while the Fukushima *et al.* (2000) model predicts a PGA of about 0.65g and the Si and Midorikawa (1999) model a PGA of 0.81g. Note that for a magnitude 5 earthquake with a focal depth of 20 km, a source distance less than 10 km may be impossible, because of the small rupture area for a magnitude 5 event.

The present study and the Si and Midorikawa (1999) study found that crustal and interface events on average produce similar PGAs. However, in the Si and Midorikawa (1999) model the PGAs from slab events are larger than those from crustal and interface events by a factor of 1.66 (Fig. 3), while the model of the present study has a factor of 1.56 for slab events at a source distance of 60 km. Their model generally predicts considerably larger PGAs than the present model. The difference is likely to come from two sources: (1) the number of events in their study was only a fraction of the number in the present study, and (2) the majority of their 127 slab event records were from two large intraplate events: 15 January 1993 off Kushiro M_w 7.6 (51 records) and 4 October 1994 east off Hokkaido M_w 8.3 event (41 records). In the present dataset, 19 records are from the 1993 event, and 10 records from 1994 event, due to distance truncation. Our residual analysis shows that the interevent errors for 4 October 1994 and 28 January 2000 events in the same area are large, and the large ground motions from these events may be a local anomaly or a particular source effect of the large slab event (see the discussion on the M_w square term in the next section). The interevent residual for the 15 January 1993 event is very small, suggesting the present model predicts the records from this event very well.

Figure 4 shows the effects of focal mechanism, tectonic source type, and focal depth on the predicted response spectra. In the present study, the base model is for crustal earthquakes with strike-slip or normal focal mechanism at a focal depth of 15 km or less. For slab events, the modification factor is distance dependent, and the scale factors for distances of 40, 60, 80, and 150 km are presented. Figure 4a shows that crustal events with a reverse focal mechanism produce about 20%–40% larger ground motions than those predicted by the base model. The reverse-fault factor is almost independent of spectral period. Abrahamson and Silva (1997) derived a magnitude-dependent reverse faulting factor that decreased with increasing period, while Sadigh *et al.* (1997) found a constant reverse model factor of 1.2 for all periods, very similar to our findings. The constant reverse faulting factor may arise from the assumption of a magnitude-independent style of faulting effect. As our base model has no magnitude-squared terms, the magnitude dependence of the reverse fault factor could not be reliably distinguished from the possible effect of neglecting magnitude-squared terms.

For PGA and spectral acceleration at 0.05-sec and 0.1-sec periods, the scale factors for interface events were set at 1.0 as the coefficients derived in the regression analysis were not statistically significant. Up to 0.4 sec, the scale factors for interface events are very small. Beyond 0.4 sec, ground motions produced by interface events decrease quickly with increasing period, and at 5.0 sec ground motions from interface events are about 60% of the motions predicted by the base model (Fig. 4a).

At a source distance of 40 km, the scale factors for slab events are over 1.6 up to 0.7 sec, and then decrease to about

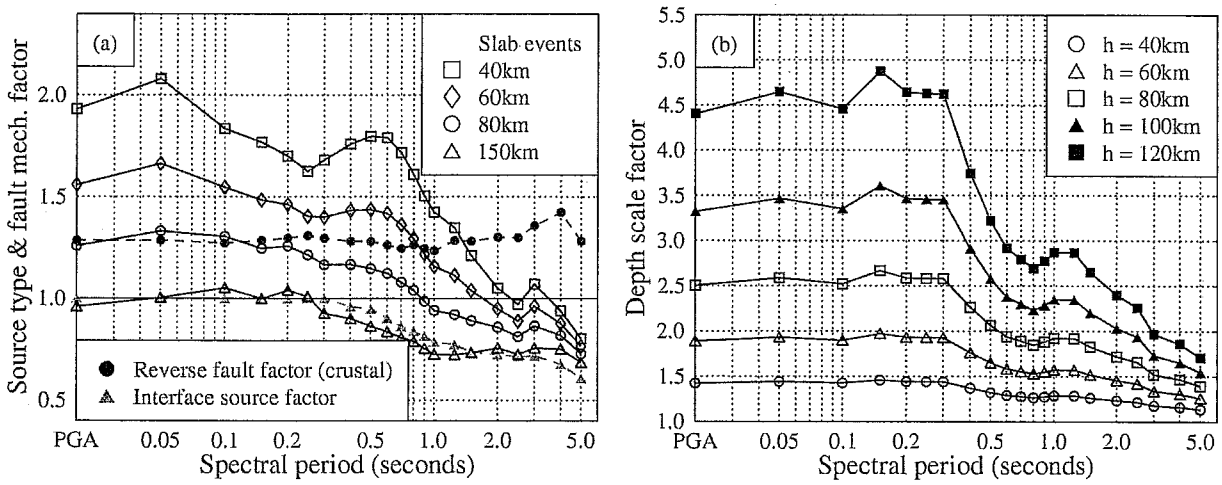

Figure 4. Scale factors for (a) source types and reverse crustal events with respect to strike-slip and normal crustal events; and for (b) focal depth with respect to events of focal depth h = 15 km or less. Note that scale factors for slab events are shown for 40-, 60-, 80-, and 120-km source distances in (a).

1.0 at a 2.0-sec period, while the scale factors at 150 km have similar values as those for interface events. Figure 4b shows the effect of focal depth for the ground motions predicted by the present model. The scale factors decrease with increasing periods beyond 0.3 sec, and the effect of focal depth is very large. However, there are very few data beyond 120 km depth (the deepest event has a focal depth of 160 km). We have no plausible explanation for the peak at about a 0.5-sec period in the scale factor for subduction events at a source distance of 60 km or less (Fig. 4a). We expect that trade-offs between the estimates of coefficients for different terms may result in such peaks. Another possibility is that the effect of depth, anelastic attenuation rate, and source-type term (all for subduction slab events) may have strong interactions. For example, the depth term may be partially a result of the large anelastic attenuation rate imposed on slab events, that is, the same anelastic attenuation rate for crustal, interface and slab events, and a part of the depth term may be a "correction" effect on the large anelastic attenuation rate (Eberhart-Phillips and McVerry, 2003). These interactions would lead to peaks in the coefficient for each term, but the predicted spectra would not be as peaked.

For the attenuation model used for a probabilistic seismic hazard study, uncertainty associated with the model has a very large effect on the level of the probabilistic ground motion. In Figure 5, comparison is made between the total prediction errors and those published previously. In order to calculate the total error for each earthquake source category, we assume that intra-event errors are independent of source category and the total error can be calculated from equation (3) by using the interevent error computed from the inter-event residuals for each earthquake category. For crustal events shown in Figure 5a, at periods less than 2.0 sec the total errors of the present study lie between the total errors from the Abrahamson and Silva (1997) model for M_w 5 and 6 events. However at periods beyond 2.5 sec, the prediction errors of the present model are markedly smaller than those for M_w 5 and 6 events and are similar to those for $M_w \geq 7$ events of the Abrahamson and Silva (1997) model.

Figure 5b shows the total errors from the Youngs *et al.* (1997) model calculated for M_w 5, 6, 7, and 8 events, and those from the present model. The total errors of the present model for subduction events are significantly smaller than those from the Youngs *et al.* (1997) model for M_w 5 and 6 events (except at the 0.1-sec period), especially for the interface events. Up to 1.5 sec, the total errors for interface events from the present study lie between those of the Youngs *et al.* (1997) model for M_w 7 and 8 events, and beyond the 2-sec period the prediction errors for both interface and slab events are markedly smaller than those for M_w 8 events. Introduction of a magnitude-squared term in our model leads to even further reduction in total prediction error (see Tables 5 and 6). The Youngs *et al.* (1997) model is based on worldwide data, and their higher prediction error may come from the regional variations in subduction zones.

Another notable feature of the present study is that the prediction errors do not generally increase with increasing period and that they actually decrease with increasing period at the long-period end. Intuitively, ground motions at long periods are less sensitive to rupture details, rapid variation of crust-velocity structure in a short distance along the wave propagating path, and even less sensitive to the variation of soil shear-wave velocity of soil sites than short-period ground motions, plausibly leading to reduction in ground-motion variability at long periods. We have processed all records in a consistent manner, and the long-period end of the usable period range has been carefully determined for each record. The consistent processing may have eliminated

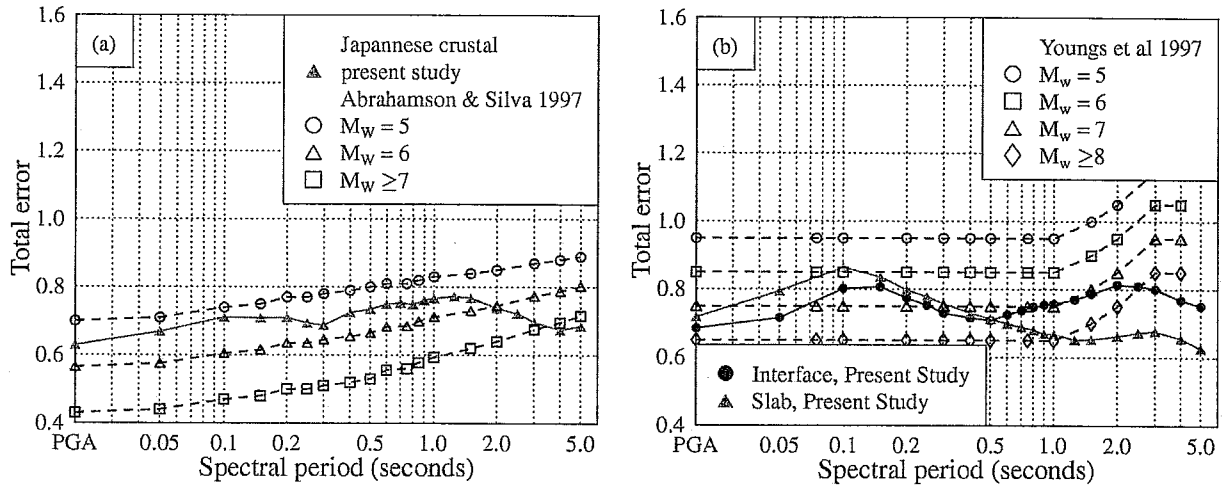

Figure 5. Total standard deviation: (a) crustal events and (b) subduction events.

Table 6
Coefficients for Magnitude Terms

Period (sec)	Q_C	W_C	τ_C	Q_I	W_I	τ_I	P_S	Q_S	W_S	τ_S
PGA	0.0	0.0	0.303	0.0	0.0	0.308	0.1392	0.1584	−0.0529	0.321
0.05	0.0	0.0	0.326	0.0	0.0	0.343	0.1636	0.1932	−0.0841	0.378
0.10	0.0	0.0	0.342	0.0	0.0	0.403	0.1690	0.2057	−0.0877	0.420
0.15	0.0	0.0	0.331	−0.0138	0.0286	0.367	0.1669	0.1984	−0.0773	0.372
0.20	0.0	0.0	0.312	−0.0256	0.0352	0.328	0.1631	0.1856	−0.0644	0.324
0.25	0.0	0.0	0.298	−0.0348	0.0403	0.289	0.1588	0.1714	−0.0515	0.294
0.30	0.0	0.0	0.300	−0.0423	0.0445	0.280	0.1544	0.1573	−0.0395	0.284
0.40	0.0	0.0	0.346	−0.0541	0.0511	0.271	0.1460	0.1309	−0.0183	0.278
0.50	−0.0126	0.0116	0.338	−0.0632	0.0562	0.277	0.1381	0.1078	−0.0008	0.272
0.60	−0.0329	0.0202	0.349	−0.0707	0.0604	0.296	0.1307	0.0878	0.0136	0.285
0.70	−0.0501	0.0274	0.351	−0.0771	0.0639	0.313	0.1239	0.0705	0.0254	0.290
0.80	−0.0650	0.0336	0.356	−0.0825	0.0670	0.329	0.1176	0.0556	0.0352	0.299
0.90	−0.0781	0.0391	0.348	−0.0874	0.0697	0.324	0.1116	0.0426	0.0432	0.289
1.00	−0.0899	0.0440	0.338	−0.0917	0.0721	0.328	0.1060	0.0314	0.0498	0.286
1.25	−0.1148	0.0545	0.313	−0.1009	0.0772	0.339	0.0933	0.0093	0.0612	0.277
1.50	−0.1351	0.0630	0.306	−0.1083	0.0814	0.352	0.0821	−0.0062	0.0674	0.282
2.00	−0.1672	0.0764	0.283	−0.1202	0.0880	0.360	0.0628	−0.0235	0.0692	0.300
2.50	−0.1921	0.0869	0.287	−0.1293	0.0931	0.356	0.0465	−0.0287	0.0622	0.292
3.00	−0.2124	0.0954	0.278	−0.1368	0.0972	0.338	0.0322	−0.0261	0.0496	0.274
4.00	−0.2445	0.1088	0.273	−0.1486	0.1038	0.307	0.0083	−0.0065	0.0150	0.281
5.00	−0.2694	0.1193	0.275	−0.1578	0.1090	0.272	−0.0117	0.0246	−0.0268	0.296

$M_C = 6.3$ and $P_C = 0.0$ for crustal and interface events, and $M_C = 6.5$ for slab events.

the unreliable part of the strong-motion records, leading to a nearly constant prediction error with respect to period.

Figure 6a shows the variation of the amplification factors, with respect to the SC I sites, for the three soil classes. The amplification factors for a particular site class are the exponential of the difference between the site class terms and SC I site class terms, for example, $\exp(C_{III} - C_I)$ for the SC III site class. The amplification curves are consistent with the definition of site class in terms of site dominant periods shown in Table 2. All three site classes show a trough at about 0.1 sec, which can be interpreted as the period of the spectral peak for SC I sites. The amplification curve for SC II sites shows a broadband amplification at periods beyond 0.15 sec. The SC III class shows a peak amplification at about 0.5 sec, which lies in the middle of dominant periods, 0.4–0.6 sec, for this site class. The amplification curve for SC IV sites has a peak at 0.9 sec that is also reasonably consistent with the definition of this site class having dominant periods larger than 0.6 sec.

The corresponding spectral shapes, that is, the spectral acceleration $S_A(T)$ (calculated from the model coefficients in Tables 4 and 5) divided by PGA, for an M_w 7.0 event at a depth of 20 km and a distance of 30 km are shown in Figure 6b for crustal strike-slip and normal-fault events and for each of the four site classes. The peak values of the spectral shapes are between 2.0 and 2.5, and the spectral periods of

the peaks increase with increasing site class, which is consistent with the site classification scheme used in the present study. For an M_w 8.0 event at a source distance of 10 km, the spectral shapes for SC I and SC II site classes have a gentle peak at about the 0.8-sec period, and the peak disappears with increasing source distance beyond 30 km. This type of bump is not unexpected considering that smoothing of the coefficients with respect to period was not performed and this effect occurs at the upper limit of the data range.

Figure 7 shows the pseudovelocity spectra for crustal, interface, and slab events for M_w 7 events at 40- and 60-km source distances. The strength of the spectra from slab events is evident, as is the reduction in elevation of the slab event spectra with increasing source distance.

Effects of Magnitude-Squared Terms

At long periods, a magnitude-squared term is often used in attenuation models for response spectra. The coefficient of this term is usually negative if moment magnitude is used (Fukushima, 1996), which means that the magnitude-squared term reduces the rate of increase in spectral amplitude with increasing magnitude for very large and great earthquakes and enhances the rate of decrease in spectral amplitude with decreasing magnitude for small earthquakes. The random-effects model used in the present study allows the partition of variability into inter- and intra-event error, and therefore the significance of the magnitude-squared term can be revealed by the analyses on the interevent residuals.

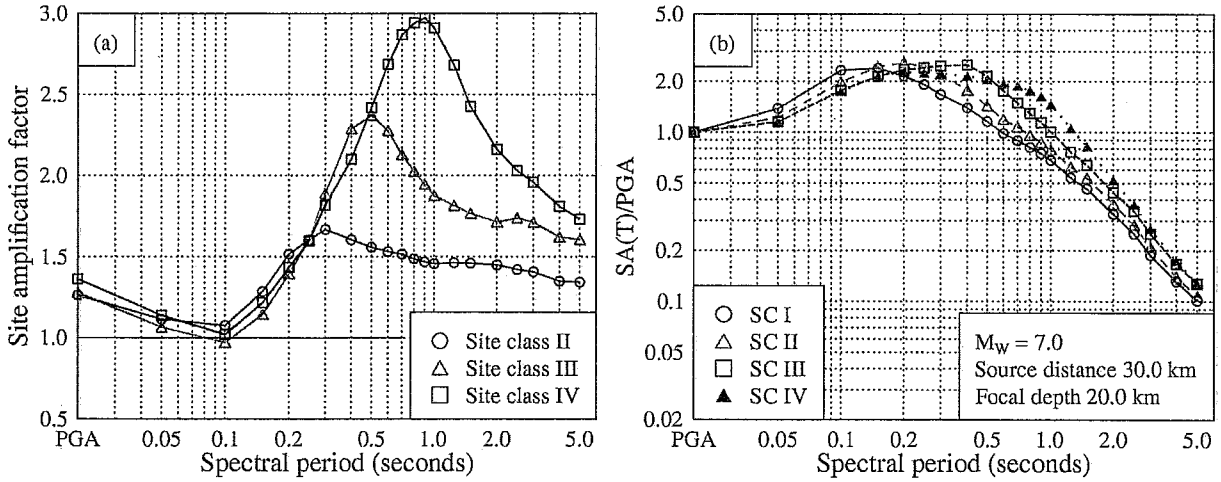

Figure 6. Illustration of site effects: (a) site amplification factors with respect to SC I sites; and (b) spectral shape for crustal strike-slip and normal events for all four site classes.

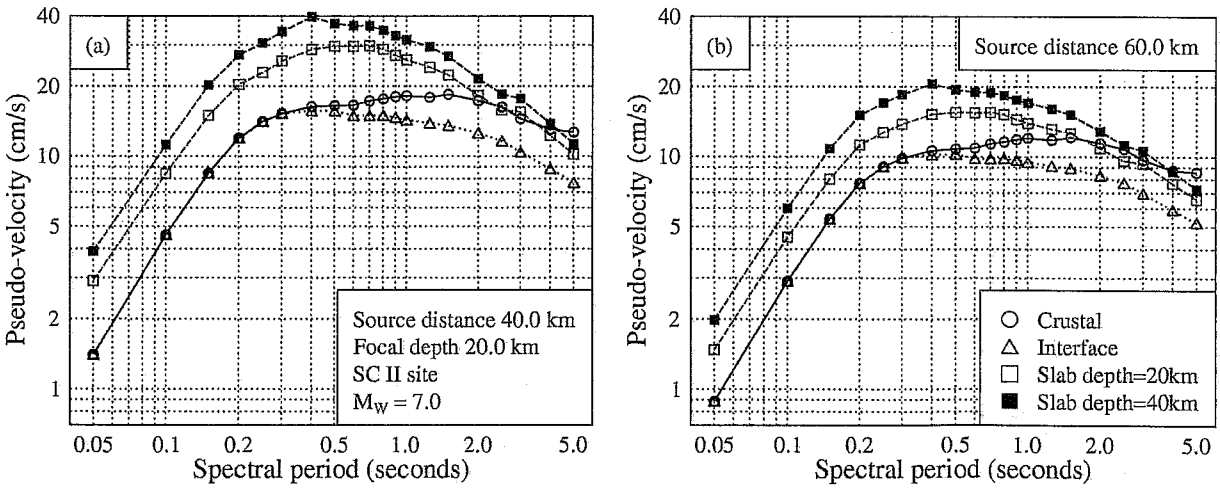

Figure 7. Pseudovelocity spectra calculated for crustal strike-slip and normal events, interface events, and slab events with a magnitude of 7.0 and a depth of 20 km for SC II sites at a source distance of (a) 40 km and (b) 60 km. The spectra from a slab event at a depth of 40 km are also presented for comparison.

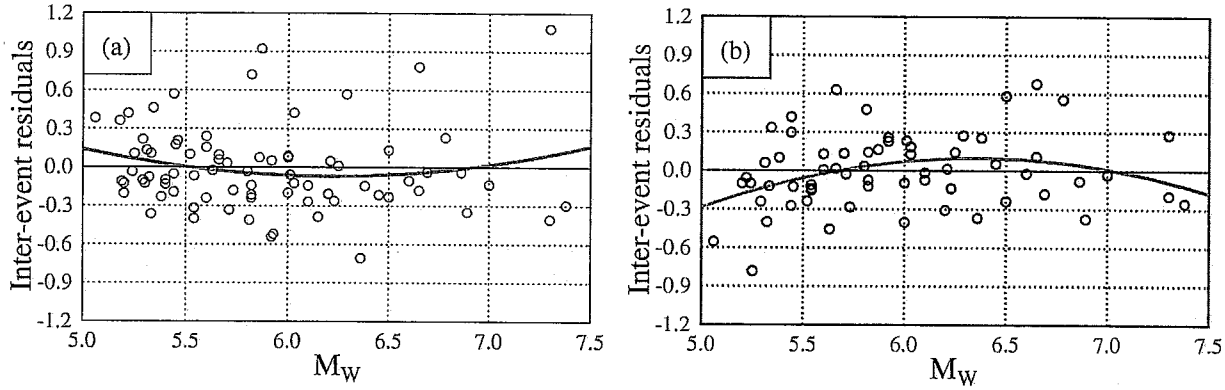

Figure 8. Interevent residuals for crustal earthquakes at (a) 0.05-sec and (b) 4.0-sec spectral periods.

The use of a magnitude-squared term in equation (1) (i.e., direct regression analyses) did not always lead to a reasonable estimate of the coefficient for the magnitude-squared term, a possible result of trade-offs between the estimates of the magnitude-squared, the linear magnitude, and the site terms. Instead, regression analyses were performed on the interevent residuals to correct the bias with respect to magnitude.

Figure 8 shows the distributions of interevent residuals with respect to magnitude for crustal earthquakes and a quadratic function of magnitude fitted to the residuals (the solid line) for 0.05-sec and 4.0-sec periods. The residuals for short-period ground motions suggest that a magnitude-squared term with a positive coefficient is required, though a linear function of magnitude fitted to the residuals would suggest no significant bias for this subset of data. It is not clear if the bias at short period is a result of the same magnitude term being used for all three earthquake source categories, or a trade-off between the estimates of other parameters. The bias with respect to magnitude for periods between 0.2 sec and 0.9 sec is negligible, while the residuals are biased moderately at long periods.

The residuals for interface events are very similar to those for the crustal events at a 4-sec period (Fig. 9). A magnitude-squared term clearly improves the modeling.

Figure 10 shows the interevent residuals of slab events for 0.05 sec, 1.0 sec, and 4.0 sec. It is possible that a magnitude-squared correction function or a function including a magnitude-cubed term could be used to reduce the bias. Investigations revealed that at short periods both types of correction functions resulted in a very similar level of correction, and at intermediate periods (up to 1.0 sec) the correction levels of the two types of functions were also very similar up to M_w 8. At periods over 2.0 sec a magnitude-squared term gave a negligible level of correction, while a function including cubic magnitude gave a considerable amount of correction around M_w 7.6 or for great earthquakes (M_w >8.3). The largest slab event in our dataset (M_w 8.25, 4 October 1994) has only 10 records, but it is this event that

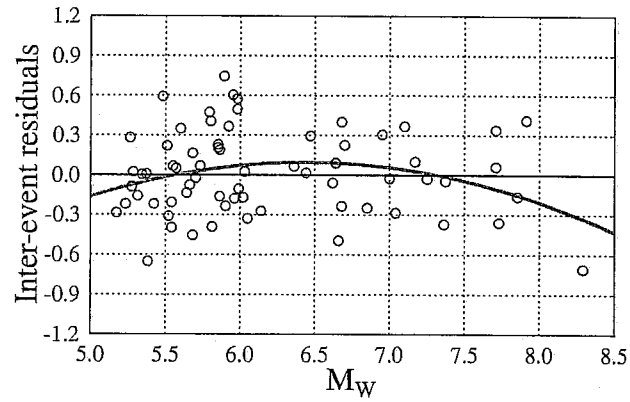

Figure 9. Interevent residuals for interface earthquakes at a 4.0-sec spectral period.

largely controls the type of correction function required. Hence, with the current data set, it is not possible to verify which correction function is the most appropriate. If a cubic-magnitude correction function is adopted, the bias at large magnitude can be better corrected. However, a cubic-magnitude correction leads to reduction of about 25% in predicted ground motions at very large magnitude, while there is only one recorded event with magnitude over 8 (Fig. 10). In order to prediction ground motions for great earthquakes in a reasonably conservative manner, we adopted the correction function using a magnitude-squared term.

In the present study, we derived a correction function from the interevent residuals of each earthquake source type separately so as to avoid the trade-offs between the estimates for the coefficient of the magnitude-squared terms for each category of earthquake. The general form of the correction term due to the effect of the magnitude-squared term is

$$\log_e(S_{MSst}) = P_{st}(M_w - M_C) + Q_{st}(M_w - M_C)^2 + W_{st}, \quad (5)$$

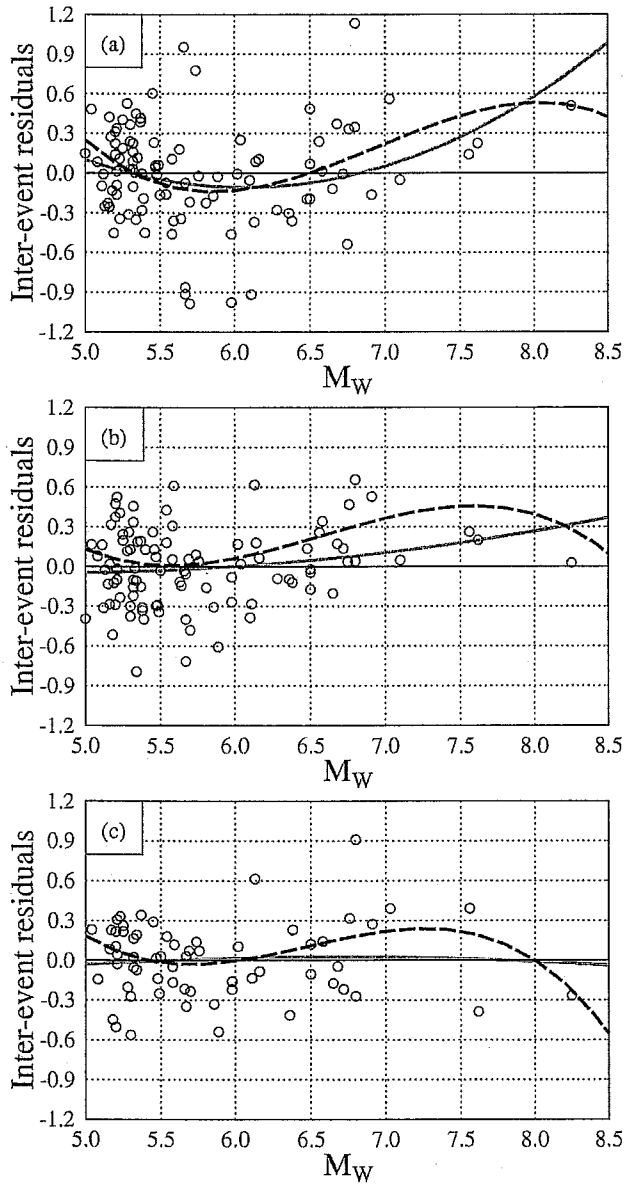

Figure 10. Interevent residuals for slab earthquakes at a 0.05-, 1.0- and 4.0-sec spectral periods.

where subscript st equals c for crustal, i for interface, and s for slab events.

The following steps were used to derive a smoothed coefficient (with respect to period) of the magnitude-squared term:

1. Fit the interevent residuals for each earthquake type to a quadratic function of $M_w - M_C$ for all periods.
2. Fit the coefficients P_{st} for $(M_w - M_C)$ and Q_{st} for $(M_w - M_C)^2$ (i.e., those derived in step 1) where subscript st denotes source types, to a function up to the fourth order of $\log_e(T)$, so that smoothed coefficients (with respect to period T) can be calculated.
3. Calculate the mean values of the differences between the residuals and the values of $P_{st}(M_w - M_C) + Q_{st}(M_w - M_C)^2$ for each earthquake (i.e., W_{st}), and fit the mean values W_{st} to a function of $\log_e(T)$.

The reason for deriving a smoothed magnitude-squared term is the consideration that even moderate peaks in the coefficients of the magnitude-squared term would lead to peaked predicted spectra. Because the effect of the magnitude-squared term for crustal and interface events is not significant at short periods when the coefficient for the magnitude-squared term is positive, the coefficients for all terms were set to zero for those cases.

The coefficients for the correction functions are presented in Table 6 together with the standard errors for the interevent residuals. The use of the correction functions leads to a reduction in the standard error. The total error for each period and each type of event can be calculated from equation (3) using the interevent errors in Table 6 and intraevent errors in Tables 4 and 5.

Figure 11a shows the correction factors due to the magnitude-squared term for crustal events. The correction factors M_w 5.5 and 7.0 are quite close to 1.0 for nearly all periods and are between 1.0 and 1.1 for M_w 6.0 and 6.5. For magnitudes 5.0 and 7.5, the correction factors are, respectively, 0.7 and 0.8 at a 5.0-sec period.

For interface events, Figure 11b shows that for M_w 5.5 and 7.0, the correction factors are very similar and are very close to unity, and that for M_w 6.0 and 6.5, the correction factors are also very similar to each other. The correction factor decreases rapidly with increasing magnitude for $M_w > 7.0$ and also decreases rapidly with increasing period for M_w 8.0 or larger.

Figure 11c shows the correction factor for slab events. It is significant only for large earthquakes ($M_w > 7.5$) and generally decreases with increasing period. The correction factors are very small at periods beyond 3 sec, and the variation with period is controlled by the functional forms of P_{st}, Q_{st}, and W_{st}.

We examined the effect of using a separate magnitude-squared term by introducing magnitude-squared terms into equation (1) and determining the coefficients simultaneously by a full regression analysis. Not surprisingly, the coefficients for the linear-magnitude terms and constant terms for source types differ moderately from those in Tables 4 and 5 and the interevent errors are either similar to those shown in Table 6 or have a marginal reduction. However, the predicted response spectra in the magnitude and distance ranges of the data set are very similar to those computed by using the coefficients in Tables 3–5. If the coefficients of all linear-magnitude terms and constants for source types (the combination of the coefficients in Tables 3–5) are fixed, the coefficients of the magnitude-squared terms derived from full regression analyses are similar to those derived separately in Table 6 for both crustal and subduction slab events at the periods where the coefficients are statistically significant.

The absolute values of the coefficients for the magnitude-squared terms derived from full regression analyses for

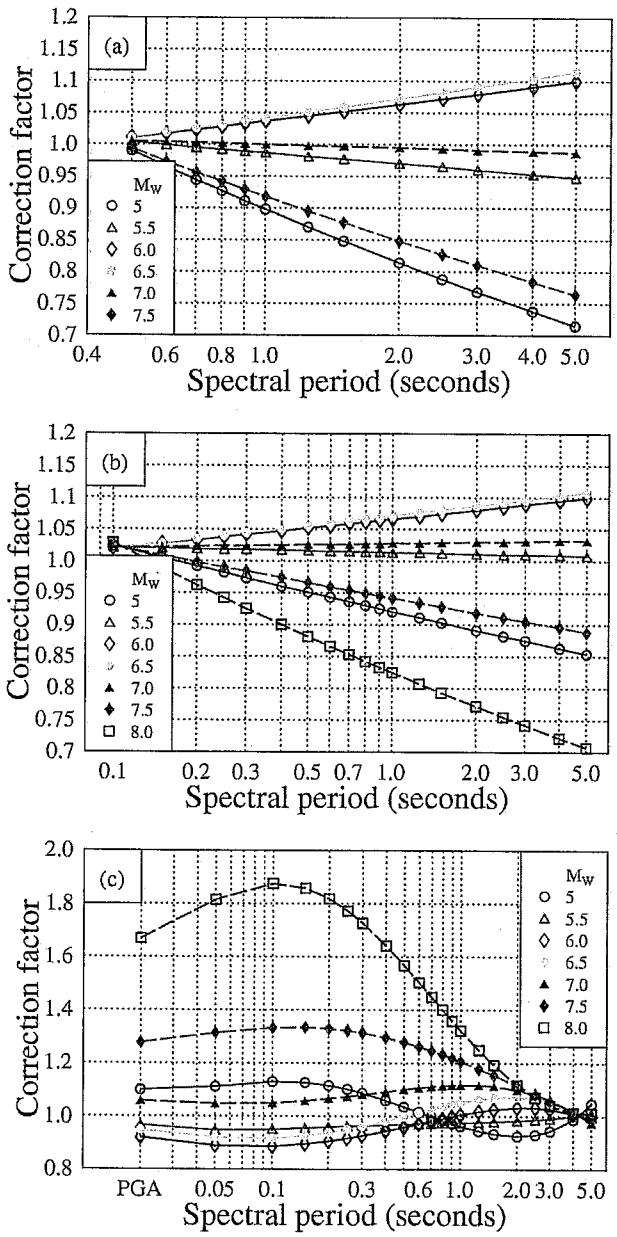

Figure 11. Scale factors derived from M_w^2 terms for (a) crustal, (b) interface, and (c) slab earthquakes.

interface earthquakes are larger than those in Table 6, and the increased values do not seem to be consistent with the interevent residuals distribution shown in Figure 9. Also the full regression analyses with magnitude-squared terms did not completely eliminate the bias of the interevent residuals with respect to the square of magnitude for all three types of earthquakes. The remaining bias is likely to be caused by the trade-offs between the estimates for the coefficients of the magnitude-squared terms for different source types and the other coefficients (all coefficients that were not fixed had minor changes after the full regression analyses). If further separate correction is applied to the interevent residuals of the full regression analyses, the total values for the coefficients of magnitude-squared terms are very similar to those presented in Table 6. The full regression shows that nearly all magnitude-squared terms that have an absolute value larger than 0.05 in Table 6 are statistically significant (at a significance level of 5%). The interevent standard errors from full regression analyses are practically the same as those presented in Table 6. These analyses suggest that the coefficients of the magnitude-squared terms derived from a separate residuals analysis are reasonable.

The coefficients in Table 6 lead to different quadratic magnitude scaling for different categories of earthquakes, and the subduction slab events require different linear-magnitude scaling than for crustal and subduction interface events. Theoretically, very long period ground motions are determined by moment magnitude, and the amplitudes of very long period ground motions should be the same for any category of earthquake that has a given moment magnitude. Possible reasons for different magnitude scaling derived in the present study are (1) the long-period end, 5-sec in our study, is still in the "short"-period range in seismological terms (Kanamori, 1986) (for magnitude determination); (2) large slab events tend to have very high stress-drops that enhance the short-period ground motions (Morikawa and Sasatani, 2004); and (3) a response spectrum at a particular period is the peak response of a single-degree-of-freedom oscillator (with a natural period equal to this particular period) subjected to ground motions associated with a wide period range around the oscillator natural period, in other word, ground motions at short period would also contribute to the response spectra at long period. The amount of contribution from short-period ground motions would depend on the relative level of ground motions at short and long periods, that is, the frequency contents (or spectral shape) of a record. For example, the relatively low long-period ground motions of subduction interface earthquakes (Fig. 4) may lead to a relatively large amount of contribution from short-period ground motions to the response spectrum at long period, compared with that for records from crustal earthquakes. These differences possibly lead to different magnitude scaling for long-period ground motions.

Discussion and Conclusions

An attenuation model accounting for tectonic source types and focal mechanisms of crustal events is derived in this study. The model predictions for all site classes and source types are plausible. The present model for crustal events predicts PGAs similar to those predicted by the Fukushima *et al.* (2000) model. Because of the much smaller prediction error of the present model, we believe that the present model is more reliable than the other models for subduction events.

The coefficients of the present model differ moderately from those of the Takahashi *et al.* (2004) model, but the predicted spectra of crustal and interface events of the two models are very similar at nearly all periods. The response

spectra predicted by the two models for slab events are also similar for source distances over 100 km. At shorter distances, however, the present model predicts significantly higher short-period spectra than the Takahashi *et al.* (2004) model.

The present model for crustal reverse-fault events predicts ground motions about 20%–40% higher than those from crustal strike-slip and normal-fault events. This result is similar to those from many other models derived from overseas crustal events. The present model also indicates that interface events produce ground motions that are similar to those of crustal strike-slip events up to 0.4 sec but produce much smaller ground motions at longer periods. At 5.0 sec, the present model predicts 30% lower ground motions for interface events than for crustal strike-slip events. The present model predicts over 60% higher ground motions for slab events at a source distance of 40 km than for crustal strike-slip events for periods up to 0.8 sec. At a 120-km distance, the spectral accelerations predicted for slab events are similar to those for the interface events. At periods beyond 0.8 sec, the spectral accelerations predicted for slab events decrease rapidly with increasing period. The difference between the factor for slab events and interface events is period- and source-distance dependent, varying from a scale factor of 2.0 at a source distance of 40 km for short and intermediate periods to a scale factor of 1.0 at all periods at a source distance of 120 km (the source-type factor for slab events at a source distance of 120 km has values very close to those of the interface event, Fig. 5a), instead of a constant of 0.364 (a scale factor of 1.44) as in the Youngs *et al.* (1997) model.

In the present model, earthquake depth has a large effect on the prediction of ground motions, especially at short periods. An earthquake at a depth of 80 km may produce ground motions 2.5 times those of an earthquake at a depth of 15 km, at the same source distance. The present model is valid for earthquakes with a depth up to 120 km.

The most important feature of the present model is that site class terms, rather than individual site terms, are used to account for site effects. This method is consistent with the methodology that is most commonly used for developing attenuation models. This approach is believed to be capable of modeling source terms without causing source effects to be shifted into individual site terms. Using site class terms is likely to retain the statistical power of ground-motion data from stations with few records.

In the present model, predictions for subduction events in the near-source region are largely constrained by shallow crustal events from the western part of the United States. Adding records within a source distance of 50 km from large earthquakes in a subduction zone with similar characteristics to those of Japan could possibly result in improved model predictions.

Residual analyses on the interevent residuals show that magnitude-squared terms are necessary for all three types of earthquakes. It is also shown that identical forms of the correction function of magnitude-squared terms can be use for both crustal and interface events, and that the magnitude-squared terms have negative coefficients, consistent with those of other studies. At short period, the correction function is close to unity for crustal and interface events. For slab events, it is possible to use magnitude-squared correction functions with or without a magnitude-cubed term. The coefficients for the magnitude-squared terms for slab events were found to be positive, which is contrary to findings of many other studies. However, the data set in the present study is very large for subduction slab earthquakes, and so the positive coefficients are well supported. The use of magnitude-squared terms generally leads to reduction of interevent standard error.

Acknowledgments

The authors thank Professor Tomotaka Iwata of DPRI, Kyoto University, and Dr. Haruko Sekiguchi of Japan Geological Survey for their generous support. We also thank Dr. Jim Cousins and Dr. David Spurr for reviewing the manuscript and their constructive comments, and Dr. Graeme McVerry for his generous support. The support from the Japanese Society for Promotion of Science for Dr. John X. Zhao during his fellowship leave in Kyoto University in 2000 is appreciated. Dr. N. Abrahamson kindly offered his computer code for the random effects model that used in the present study. The constructive comments from two anonymous reviewers are greatly appreciated. We would like to acknowledge a number of organizations who kindly provided us the strong-motion data: Building Research Institute, California Division of Water Resources, California Strong Motion Instrumentation Program, Central Research Institute of Electric Power Industry, Hanshin Expressway Public Corporation, Honshu-Shikoku Bridge Authority, Japan Meteorological Agency, JR Group, Kansai Electric Power Company, Kobe City Office, Kyoto University, Maeda Corporation, Matsumura-gumi Corporation, Ministry of Internal Affairs and Communications, National Institute for Land and Infrastructure Management, National Research Institute for Earthquake Science and Disaster Prevention (K-net and KiK-net); Obayashi Corporation, Osaka Gas Co., Ltd., Port and Airport Research Institute, Railway Technical Research Institute, Shiga Prefecture, Association for Earthquake Disaster Prevention, Committee of Earthquake Observation and Research in the Kansai Area, University of Shiga Prefecture, Tokyo Electric Power Company, United States Geological Survey, Urban Renaissance Agency (alphabetical order).

References

Abrahamson, N. A., and W. J. Silva (1997). Empirical response spectral attenuation relations for shallow crustal earthquakes, *Seism. Res. Lett.* **68,** 94–127.

Abrahamson, N. A., and R. R. Youngs (1992). A stable algorithm for regression analysis using the random effect model, *Bull. Seism. Soc. Am.* **82,** 505–510.

Building Seismic Safety Council (2000). *The 2000 NEHRP Recommended Provisions for New Buildings and Other Structures: Part I (Provisions) and Part II (Commentary)*, FEMA 368/369, Federal Emergency Management Agency, Washington, D.C.

Eberhart-Phillips, D., and G. McVerry (2003). Estimating slab earthquakes response spectra from a 3D Q model, *Bull. Seism. Soc. Am.* **93,** 2649–2663.

Engdahl, E. R., R. D. Van der Hilst, and R. P. Buland (1998). Global teleseismic earthquake relocation with improved travel times and procedures for depth determination, *Bull. Seism. Soc. Am.* **88,** 722–743.

Fukushima, Y. (1996). Scaling relations for strong ground motion prediction models with M2 term, *Bull. Seism. Soc. Am.* **86,** 329–336.

Fukushima, Y., and T. Tanaka (1990). A new attenuation relation for peak horizontal acceleration of strong earthquake ground motion in Japan, *Bull. Seism. Soc. Am.* **80,** 757–783.

Fukushima, Y., K. Irikura, T. Uetake, and H. Matsumoto (2000). Characteristics of observed peak amplitude for strong ground motion from the 1995 Hyogo-ken Nanbu (Kobe) earthquake, *Bull. Seism. Soc. Am.* **90,** 545–565.

Hauksson, E. (2000). Crustal structure and seismicity distribution adjacent to the Pacific and North America plate boundary in southern California, *J. Geophys. Res.* **105,** 13,875–13,903.

Kanamori, H. (1986). Rupture process of subduction-zone earthquakes, *Annu. Rev. Earth Planet. Sci.* **14,** 293–322.

Kobayashi, S., T. Takahashi, S. Matsuzaki, M. Mori, Y. Fukushima, J. X. Zhao, and P. G. Somerville (2000). A spectral attenuation model for Japan using digital strong motion records of JMA87 type, Presented at 12th World Conference of Earthquake Engineering, 2000, Auckland, New Zealand.

Molas, G. L., and F. Yamazaki (1995). Attenuation of earthquake ground motion in Japan including deep focus events, *Bull. Seism. Soc. Am.* **85,** 1343–1358.

Morikawa, N., and T. Sasatani (2004). Source models of two large intraslab earthquakes from broadband strong ground motions, *Bull. Seism. Soc. Am.* **94,** 803–817.

Sadigh, K., C.-Y. Chang, J. A. Egan, F. Makdisi, and R. R. Youngs (1997). Attenuation relationships for shallow crustal earthquakes based on Californian strong motion data, *Seism. Res. Lett.* **68,** 180–189.

Si, H., and S. Midorikawa (1999). New attenuation relationships for peak ground acceleration and velocity considering effects of fault type and site condition, *J. Struct. Construct. Eng. AIJ* **523,** 63–70.

Takahashi, T., T. Saiki, H. Okada, K. Irikura, J. X. Zhao, J. Zhang, H. K. Thoi, P. G. Somerville, Y. Fukushima, and Y. Fukushima (2004). Attenuation models for responsespectra derived from Japanese strong-motion records accounting for tectonic source types, paper 1271, Presented at 13th World Conference of Earthquake Engineering, 2004, Vancouver, B.C., Canada.

Youngs, R. R., S.-J. Chiou, W. J. Silva, and J. R. Humphrey (1997). Strong ground motion attenuation relationships for subduction zone earthquakes, *Seism. Res. Lett.* **68,** 94–127.

Zhao, J. X., K. Irikura, J. Zhang, Y. Fukushima, P. G. Somerville, T. Saiki, H. Okada, and T. Takahashi (2004). Site classification for strong-motion stations in Japan using h/v response spectral ratio, paper 1278, Presented at 13th World Conference of Earthquake Engineering, 2004, Vancouver, B.C., Canada.

Institute of Geological and Nuclear Sciences
Lower Hutt, New Zealand
(J.X.Z, J.Z.)

Shikoku Electric Power Co., Inc.
Takamatsu, Japan
(A.A., Y.O., T.O., T.T., H.O.)

Aichi Institute of Technology
Japan
(K.I.)

URS Corporation
Pasadena, California 91101-2506
(H.K.T, P.G.S.)

Japan Engineering Consultants Co., Ltd.
Tokyo, Japan
(Ya.F.)

Ohsaki Research Institute Co., Inc.
Japan
(Yo.F.)

Manuscript received 13 June 2005.